Optics and Photonics

9 Actively Mode-locked Linear Fiber Laser

Sponsors

US Air Force Office of Scientific Research
Grant F4920-98-1-0139
Air Force Office of Scientific Research (Defense Advanced Research Projects Agency)
Grant F49620-96-0126

Project Staff

Erik R. Thoen, Matthew E. Grein, Elisabeth M. Koontz, Professor Erich P. Ippen, Professor Leslie A. Kolodziejski

Active harmonic mode-locking is particularly attractive for communication systems which require a high bit-rate locked to an external clock. However, most such lasers are implemented in a ring geometry where pulses pass through the modulator in only one direction. A linear laser has several advantages such as the possibility of integration, the simple incorporation of a semiconductor saturable absorber mirror, and the feasibility of environmental stability through Faraday rotation. But in a linear laser, modulation of the pulse traveling in the direction opposite to that of the traveling wave modulation signal can produce loss and affect timing. In this work we demonstrate modelocking of a linear harmonically mode-locked fiber laser with a traveling-wave phase modulator, and show that for frequencies greater than the inverse of twice the transit time through the modulator, the phase modulation on the counter-propagating wave can be insignificant.

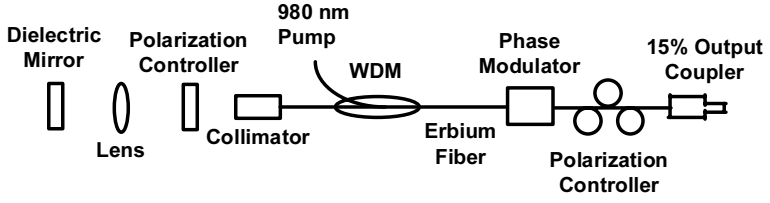

Figure 13. Schematic of the actively modelocked linear laser Wavelength Division Multiplexer (WDM).

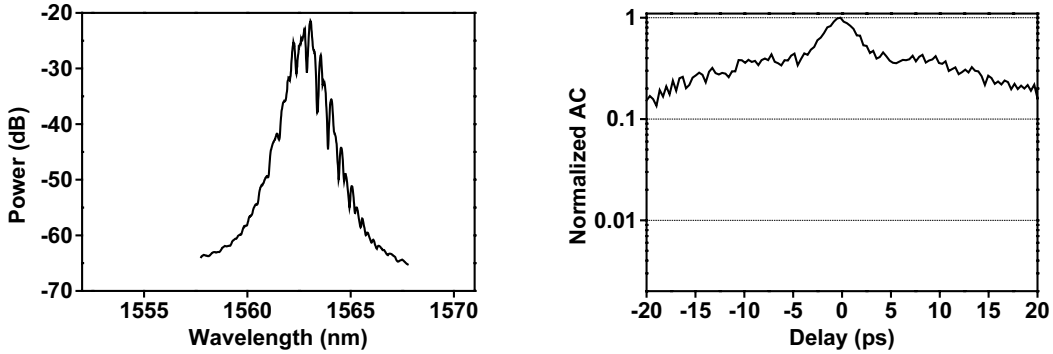

Figure 14. Spectrum and autocorrelation for operation at a low harmonic

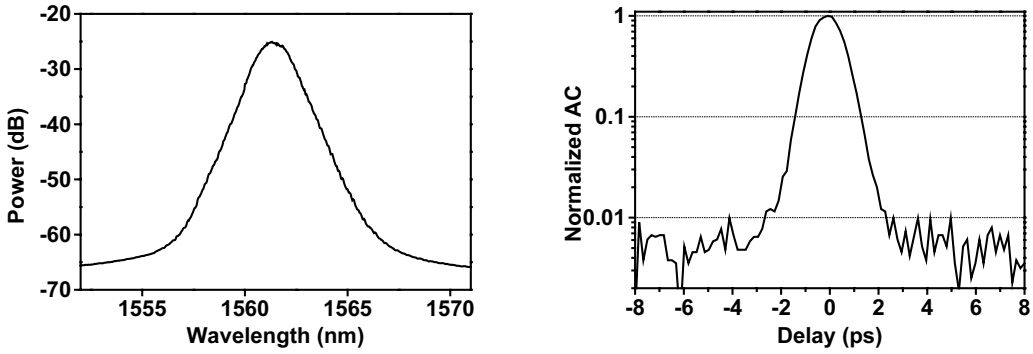

Figure 15. Spectrum and autocorrelation for high-harmonic operation.

The laser shown in Fig. 13 was constructed with an anomalous round-trip cavity dispersion of -0.07 ps^2. When the modulator was operated at low frequencies (100-500 MHz), the laser produced the optical spectrum and autocorrelation shown in Fig. 14. The spectrum displays significant modulation, and the autocorrelation indicates a very long background pulse. These frequencies are far below the traveling-wave regime, so the modulator imparts a significant phase shift on the counter-propagating light. When the modulator frequency is increased to 4 GHz, well above the traveling-wave frequency, the spectrum and autocorrelation shown in Fig. 15 were produced. The modulation is absent from the spectrum, and the picosecond pulse is clean over a high dynamic range.

Publications

Thoen, E.R., M. E. Grein, E. M. Koontz, L. A. Kolodziejski, and E. P. Ippen. "Active Harmonic Mode-locking of a Linear Fiber Laser Assisted by a Semiconductor Saturable Absorber Mirror." Paper presented at the Optical Society of America Annual Meeting, Santa Clara, CA, September 1999.

10 Noise Studies in Harmonic, Actively Modelocked Fiber Lasers

Sponsors

US Air Force Office of Scientific Research
Grant F4920-98-1-0139
Air Force Office of Scientific Research (Defense Advanced Research Projects Agency)
Grant F49620-96-0126
Air Force Office of Scientific Research (Defense Advanced Research Projects Agency)
Lincoln Laboratory (PACT)

Project Staff

Matthew E. Grein, Leaf. A. Jiang, Dr. Yijiang Chen, Professor Erich Ippen, Professor Hermann A. Haus

The low-timing jitter performance of actively modelocked fiber lasers makes them suitable candidates as optical clocks for precision, high-speed optical analog-to-digital converters. Much of the low-noise performance, relative to semiconductor lasers, arises from the long upper-state lifetime of the rare-earth dopants in the amplifier that integrates over intensity dynamics. The jitter is caused by perturbations due to spontaneous emission noise and is damped by time constants related to laser parameters such as modulation depth, filtering, and group-velocity

dispersion (GVD). The purpose of our study is twofold: to develop a stable, active, harmonically modelocked fiber laser producing picosecond pulses at 10 GHz, and to measure the characteristic time constants governing pulse retiming in the laser, both for AM and PM operation.

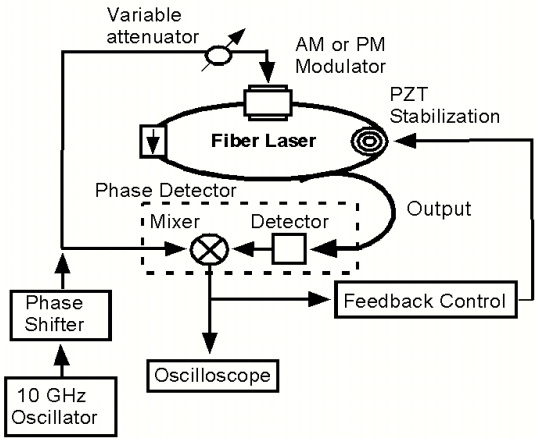

Figure 16. Laser configuration.

The laser we have developed is shown in Figure. 16. The fiber laser is 167 meters long--corresponding to a 1.2 MHz free spectral range (833 ns round trip time)--and constructed with polarization-maintaining fibers. The pulsewidth can be varied from 1.5 to 3.5 ps by changing the pump power and modulation depth. The rf synthesizer is set to the frequency of the cavity harmonic closest to 10 GHz, and suppression of the supermodes is greater than 65 dB. The laser pulse train is detected with a photodiode (45 GHz electrical bandwidth), and the phase of the fundamental component is compared to the rf synthesizer driving the modulator, generating an error signal. The error signal is integrated and amplified to drive a fiber-wound PZT that changes the length of the laser cavity, completing a phase-locked feedback loop that ensures stable active modelocking.

By applying an instantaneous perturbation to the phase of the rf synthesizer driving the laser and opening the feedback circuit--achieved in practice by reducing the bandwidth of the feedback circuit to less than 2 Hz so as to maintain stable modelocking during repeated measurements—we obtain the transient retiming dynamics at the output of the phase detector. The theory we developed predicts that the recovery for AM should exhibit an exponential recovery proportional to the length of the laser and inversely proportional to the product of the modulation depth and square of the pulsewidth. For PM, the timing recovery is described as that of a damped harmonic oscillator.

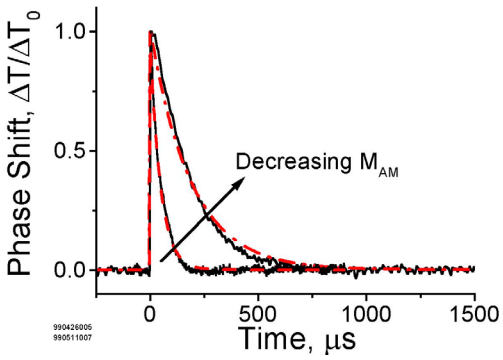

Figure 17: Timing recovery following a step-wise excitation, amplitude modulation.

Traces of the retiming dynamics after an instantaneous phase shift are shown in Figure 17 for two different modulation depths. The dashed and dashed-dot lines are fits to an exponential decay. The recovery times for the two traces are 45 and 175 μs, corresponding to 54 and 210 round trips, respectively. A series of such traces was taken for various values of modulation depth, and the recovery time was extracted for each corresponding exponential fit. The measured time constants for AM are in excellent agreement with the theory: the recovery time is proportional to the length of the cavity and inversely proportional to the product of the modulation depth, square of the modulation frequency, and square of the pulsewidth.

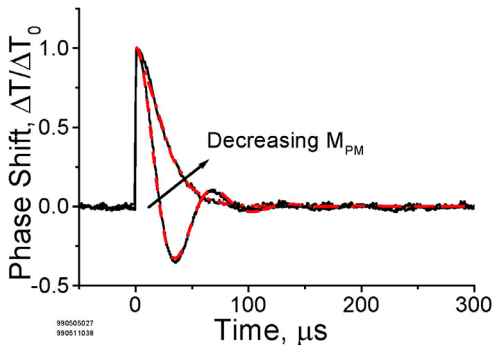

Figure 18: Timing recovery following a step-wise excitation, phase modulation.

In contrast to the case of AM, timing is not restored directly by PM. Mistimed pulses first experience a shift in frequency that converts to retiming through group-velocity dispersion (GVD). Upon successive round trips, the accumulated frequency shifts are damped out by filtering. Two typical traces are shown in Figure 18, one corresponding to the underdamped case (where the modulation depth is large) and another where the retiming follows a trajectory closer to that for critical damping (where the modulation depth has been reduced). The curve fits correspond to a damped harmonic oscillator with two free parameters. The measured time constants are in excellent agreement with the theory: timing recovery for PM is governed by two time constants, one governing damping, and another governing oscillation.

These dynamics studies have confirmed the qualitative and quantitative theory of the noise in actively modelocked fiber lasers. In conjunction with the theory, our preliminary results indicate that the minimum jitter for AM requires dispersion management in which the local dispersion swings between anomalous and normal, but the net dispersion is near zero. This reduces the jitter due to frequency fluctuations while enhancing the pulse energy. For PM, the minimum jitter requires an optimum dispersion because large dispersion increases the timing recovery from noise that comes from timing fluctuations, but dispersion also increases the noise that comes from frequency shifts via the Gordon-Haus effect.

Publications List

Grein, M.E., L.A. Jiang, Y. Chen, H.A. Haus, and E.P. Ippen, “Timing Restoration Dynamics in an Actively Mode-Locked Fiber Ring Laser,” *Opt. Lett.* 24: 1687-89 (1999)

Grein, M.E., L.A. Jiang, Y. Chen, H.A. Haus, and E.P. Ippen. “A Study of the Dynamics Governing Timing Restoration in the Actively Modelocked Soliton Laser.” Paper presented at the Conference on Lasers and Electro-Optics (CLEO’99), Optical Society of America, Baltimore, MD, paper CtuJ1,May 23-28, 1999.

11 Phase Jitter in Modelocked Semiconductor Lasers

Sponsor

Air Force Office of Scientific Research (Defense Advanced Research Projects Agency)
Lincoln Laboratory (PACT)

Project Staff

Leaf A. Jiang, Mathew E. Grein, Professor Erich P. Ippen, Professor Herman A. Haus

The carrier phase noise in cw semiconductor lasers has been analyzed theoretically and measured experimentally[1]. The noise of a mode-locked laser diode (MLLD) can be broken into four orthogonal fluctuations: energy, carrier phase, frequency, and timing. In this paper, we measure the carrier phase noise as well as the energy fluctuations of a bi-section monolithically integrated 45 GHz repetition rate MLLD[2] and compare it to theory. The width of pulses are 1.3 ps, the overall length of the laser diode is 960 μm (driven at 38.2 mA), and the length of the saturable absorber section is 60 μm (biased at 0.225 V).

The power spectrum of the directly-detected output of the MLLD is the convolution of the linewidth of the laser, a sum of delta functions spaced by the 45 GHz repetition rate, and the relaxation-oscillation spectrum of the laser-diode. The amplitude of the relaxation-oscillation spectrum is related to the intensity noise. Since the relaxation-oscillation is in the few-GHz range (2.2 GHz in our case), a 3 GHz photodetector was used to measure its spectrum (see Fig. 19). The intensity noise variance was estimated by fitting the experimental relaxation-oscillation spectrum to a second-order theoretical curve[3] that upperbounds the variance but does not take into account asymmetries that may be due to higher order nonlinearities, coupling between amplitude and phase, or saturable absorber dynamics. The intensity noise variance was 22 μW^2 for an average detected power of 415 μW.

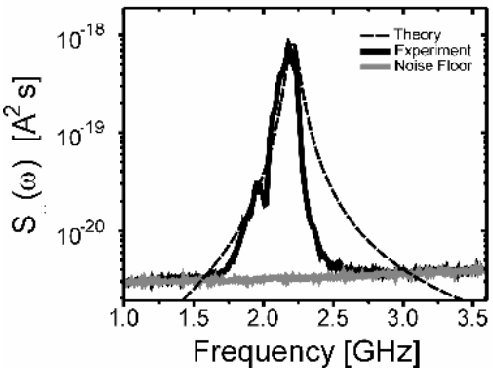

Figure 19. RF spectrum of the MLLD. The amplitude noise has a peak at the relaxation oscillation frequency of 2.2 GHz. The gray line shows the noise floor of the RF spectrum analyzer.

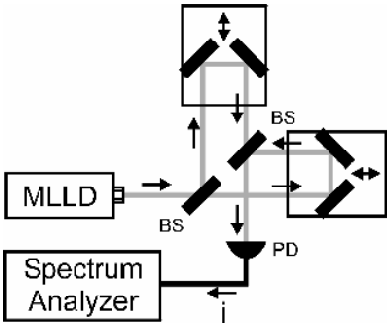

Figure 20. Experimental setup. BS is beam splitter; PD is photodetector.

The experimental setup used to measure the pulse-to-pulse carrier phase noise is shown in Fig. 20 and is similar to that of Piazzolla et al.[2] One arm of the interferometer is delayed so that neighboring pulses overlap on the detector, and the photocurrent is displayed on an RF spectrum analyzer. Both phase and amplitude noise have peaks at the relaxation oscillation frequency of the MLLD and can be distinguished in the power spectrum of the photocurrent by suitable biasing of the interferometer. Assuming that the intensity and phase noise are independent, the power spectrum of the photocurrent consists of four parts: a DC term, a term for the phase noise, a term for intensity noise, and a term due to mixing of phase and intensity noise. The terms corresponding to the intensity noise are determined by the direct-detection measurement described in the previous paragraph. Using the variance of the pulse-to-pulse phase difference as the only fitting parameter, the theoretical spectrum (drawn with a dashed line in Fig. 21) is fitted to the experimental data (drawn with a solid line), yielding a value of 0.014 rad^2. The ripples in the experimental curve reflect fluctuations of the laser power and interferometer on the time scale of the RF spectrum analyzer sweep rate (200 ms).

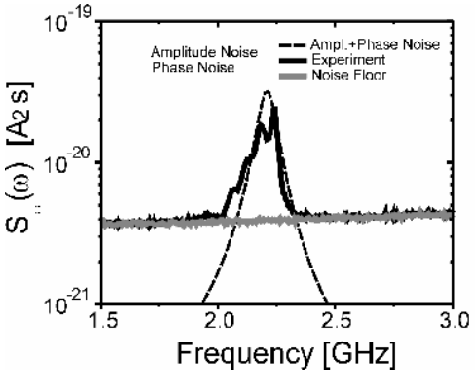

Figure 21. RF spectrum of the output from the Michelson interferometer biased for maximum sensitivity to phase noise. The noise is due to both amplitude and phase fluctuations of the laser.

References

1 S. Piazzolla, P. Spano, and M. Tamburrini, "Characterization of phase noise in semiconductor lasers," *Appl. Phys. Lett.* 41: 695-96 (1982).

2 X.-L. Wang, H. Yokoyama, and T. Shimizu, "Synchronized harmonic frequency mode-locking with laser diodes through optical pulse train injection," *IEEE Photon. Tech. Lett.* 8: 617 (1996).

3 G. P. Agrawal, and N. K. Dutta, *Long-Wavelength Semiconductor Lasers* (Van Nostrand Reinhold Company, 1986), Chap. 6.

Publications List

L. A. Jiang, M. E. Grein, E. P. Ippen, H. A. Haus, T. Shimizu, H. Kurita, and H. Yokoyama. “Noise measurements of a 45 GHz mode-locked laser diode,” to be presented at CLEO ’00, San Francisco, CA, May 2000.

12 Mode-locking Stability with Two-Photon Absorption and Free-Carrier Absorption

Sponsors

US Air Force Office of Scientific Research
Grant F4920-98-1-0139
Air Force Office of Scientific Research (Defense Advanced Research Projects Agency)
Grant F49620-96-0126

Project Staff

Erik. R. Thoen, Elisabeth M. Koontz, Thomas R. Schibli, Dr. Markus Joschko, Dr. Patrick Langlois, Dr. Franz X. Kärtner, Professor Erich P. Ippen, Professor Leslie A. Kolodziejski

Semiconductor saturable absorber mirrors are used to mode-lock a wide range of both solid-state and fiber lasers. Recent investigations by our group into the nonlinear dynamics of such mirrors have revealed the presence of two-photon absorption (TPA) and nonlinear free-carrier absorption (FCA) at fluence levels which occur routinely in mode-locked lasers. The purpose of this study is to evaluate the effect that these nonlinearities can have on the stability of continuous-wave mode-of the locking.

The effect of TPA on mode-locking stability can be assessed by modifying the expressions typically used for saturable absorption and applying a perturbational stability analysis. The condition for stability of continuous-wave mode-locking (CWML) against Q-switched mode-locking (QSML), is applied, with the effect of TPA in the saturable absorber. Fast saturable absorption, TPA, loss, and gain saturation are all included in the stability analysis of the CWML state against perturbations. Figure 22 illustrates the calculated stability regions in a normalized logarithmic plot of the saturation power of the absorber versus the pulse energy, ($I_A A_A / I_L A_L$) versus (W/W_L), where A_A is the area of the spot focussed on the absorber, I_L is the saturation intensity of the gain, A_L is the area of the beam in the gain medium, W is the pulse energy, and $W_L = I_L A_L T_R$ where T_R is round-trip time of the cavity. [The normalized pulse energy scales with pump power ($W/W_L = 0$ at the threshold of lasing).] For the stability calculation the full-width half-maximum pulsewidth for a sech-shaped pulse is 264 fs and $q_o T_L = 4.1 \times 10^4$, where T_L is the upperstate gain lifetime normalized to the cavity round-trip time. The solid line in Figure 22 indicates the instability boundary when TPA is not included; the inclusion of TPA reduces the instability boundary to the dashed line. Quite clearly the region of stability is greatly increased in terms of both pulse energy and absorber saturation when TPA is present in the absorber structure. The analysis demonstrates that TPA can enable a laser to reach a CWML state that was not previously attainable. FCA, as a pulse energy dependent loss mechanism, produces similar mode-locking stabilization. Therefore, appropriate use of TPA and FCA may lead to dramatic improvements in stabilization against QSML for many laser systems.

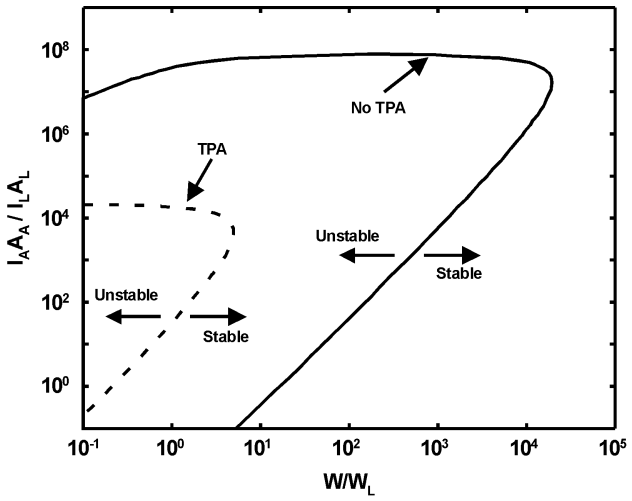

Figure 22. Calculated stability contours for a fast saturable absorber mode-locked laser. QSML is present in the regions labeled "unstable". CWML is present in the regions labeled "stable". The area within the solid line is the instability region without TPA included in the model. The area within the dashed line is the instability region with TPA included in the model.

Publications

Schibl, T.R., E.R. Thoen, F.X. Kärtner, and E.P. Ippen. "Suppression of Modelocked Q-Switching and Break-Up into Multiple Pulses by Inverse Saturable Absorption." Submitted to *Appl. Phys. B*.

Thoen, E.R., E.M. Koontz, D.J. Jones, D. Barbier, F.X. Kärtner, E.P. Ippen, and L.A. Kolodziejski. "Erbium-Ytterbium Waveguide Laser Mode-Locked with a Semiconductor Saturable Absorber Mirror." *IEEE Photon. Technol. Lett*. 12: 149-51 (2000).

Schibli, T.R., E.R. Thoen, E.M. Koontz, F.X. Kärtner, E.P. Ippen, and L.A. Kolodziejski. "Suppression of Modelocked Q-Switching and Multiple Pulse Break-up by Two-Photon Absorption." Poster presentation given July 11-16, 1999 at the Ultrafast Optics Meeting, Ascona, Switzerland.

Thoen, E.R., E.M. Koontz, M. Joschko, P. Langlois, T.R. Schibli, F.X. Kärtner, E.P. Ippen, and L.A. Kolodziejski. "Two Photon Absorption in Semiconductor Saturable Absorber Mirrors." *Appl. Phys. Lett*. 74: 3927-29 (1999).

13 Stabilization of Active, Harmonically Modelocked Fiber Lasers using Two-Photon Absorbers

Sponsors

Air Force Office of Scientific Research (Defense Advanced Research Projects Agency)
Lincoln Laboratory (PACT)
Air Force Office of Scientific Research (Defense Advanced Research Projects Agency)
Grant F49620-96-0126
US Air Force Office of Scientific Research
Grant F4920-98-1-0139

Project Staff

Matthew E. Grein, Erik R. Thoen, Elizabeth M. Koontz, Professor Erich P. Ippen, Professor Hermann A. Haus, Professor Leslie A. Kolodziejski

Active harmonically mode-locked fiber lasers producing picosecond pulses at gigahertz repetition rates for communications and precision optical sampling require a mechanism to equalize pulse energies to prevent amplitude fluctuations and pulse dropouts. We showed previously that two photon absorption (TPA) can limit the peak intensity of Q-switched mode-locking and enhance the stability of continuous-wave mode-locking[1]. In this work, we show that a semiconductor mirror providing TPA in a harmonically mode-locked fiber laser introduces a fast intensity-dependent loss that can equalize pulse energies and reduce pulse dropouts.

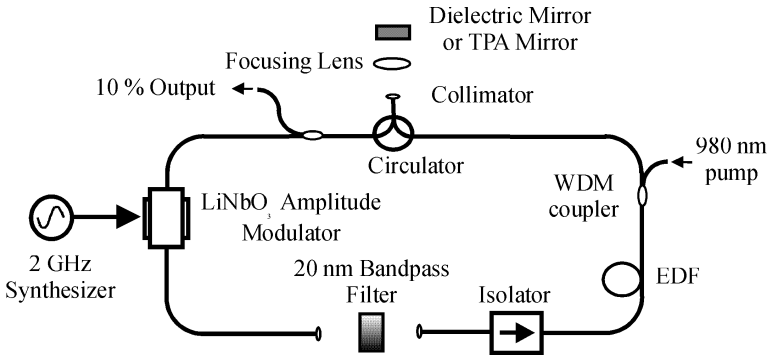

Figure 23. Laser setup; all fibers are polarization maintaining.

Figure 23 shows a ~ 47 m active harmonically mode-locked fiber laser operating at 2 GHz. The average group-velocity dispersion is ~ 6 ps/nm/km (anomalous). The fibers are polarization maintaining to eliminate nonlinear polarization effects. A circulator incorporates a mirror in the ring cavity. An aspheric lens is used to produce a small spot size (~ 5×10^{-8} cm^2) on the mirror. To test the laser operation without TPA, a dielectric mirror (> 99.9% reflectivity at 1.55 μm) was used in this position. Autocorrelations yielded transform-limited 1.8 ps pulses at 1.555 μm. The rf spectrum exhibited 25 dB supermode suppression, as shown in Figure 24a, indicative of occasional dropouts. Figure 24b shows a digital oscilloscope scan over a long time scale (tens of ns) as compared to the repetition rate (500 ps), verifying that pulses are missing. Note that individual pulses are not resolved due to the limited resolution of the oscilloscope.

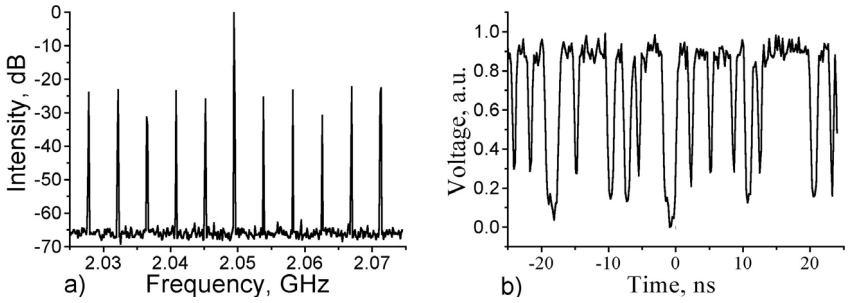

Figure 24. Laser output without the TPA mirror. a) Rf power spectrum, 3 kHz resolution bandwidth, and b) Digitizing oscilloscope trace.

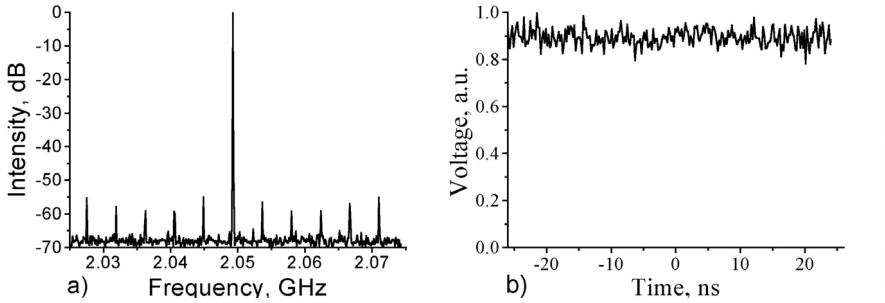

Figure 25. Laser output with the TPA mirror and focusing lens. a) Rf power spectrum, 3 kHz resolution bandwidth, and b) Digitizing oscilloscope trace.

The dielectric mirror was replaced by a TPA mirror, and with the average power held constant, the laser produced pulses of similar duration. The TPA mirror consists of a ~5.1 μm InP layer deposited via gas source molecular beam epitaxy onto a 22 period GaAs/AlAs distributed Bragg reflector (>99% reflectivity at 1.55 μm). A dielectric antireflection coating was deposited on the front surface. TPA introduces an instantaneously greater loss for higher peak intensity, which suppresses amplitude fluctuations and pulse dropouts by favoring a filled pulse train of low-intensity pulses over a partially filled pulse train of high-intensity pulses. The supermode suppression shown in Figure 25a was enhanced by 30 dB (compared with Figure 24a), and the corresponding oscilloscope trace in Figure 25b reveals the absence of pulse dropouts. Based on nonlinear reflectivity measurements of a similar structure and the incident peak intensity, the nonlinear loss of the TPA mirror was estimated to be between 0.5 and 1% for the pulses described above. To verify the intensity dependence of the TPA effect, the peak intensity on the TPA mirror was lowered dramatically by removing the focusing lens (spot size ~ 9.5×10^{-3} cm^2), yielding results similar to those of Figure 24.

Some of the novel features of TPA-assisted harmonic mode-locking are the enabled operation of environmentally stable, short laser cavities; the potential for specific tailoring of semiconductor materials and waveguide structures for optimum performance and integration; and laser operation even in the non-soliton regime.

References

1 T.R. Schibli, E.R.Thoen, F.X. Kärtner and E.P. Ippen, “Suppression of Modelocked Q-Switching and Break-Up into Multiple Pulses by Inverse Saturable Absorption,” Appl. Phys. B, forthcoming.

Publications

Grein, M.E., E.R. Thoen, E.M. Koontz, H.A. Haus, L.A. Kolodziejski, and E.P. Ippen, “Stabilization of an Active Harmonically Mode-Locked Fiber Laser using Two-Photon Absorption”, To be presented at the 2000 Conference on Lasers and Electro-Optics, San Francisco, California, May 7-12, 2000.

14 Soliton Fiber Laser with Saturable Absorber Mode-locking

Sponsors

US Air Force Office of Scientific Research
Grant F4920-98-1-0139
Air Force Office of Scientific Research (Defense Advanced Research Projects Agency)
Grant F49620-96-0126

Project Staff

Erik R. Thoen, Elisabeth M. Koontz, Dr. Franz X. Kärtner, Professor Erich P. Ippen, Professor Leslie A. Kolodziejski, Professor Hermann A. Haus

Passively mode-locked fiber lasers relying on polarization rotation are frequently difficult to self-start and often sensitive to environmental changes. Linear fiber laser geometries present a particular challenge due to standing wave effects. In these cases semiconductor saturable absorber mirrors provide an attractive mechanism for starting and maintaining modelocking. They also have the advantages of compact size, environmental stability, and simplicity. In this work we are investigating the modelocking of linear fiber lasers with a variety of dispersion maps using a semiconductor saturable absorber mirror. This mirror consisted of an anti-reflection-coated $\lambda/2$ InP-based absorber structure deposited by gas source molecular beam epitaxy on a distributed Bragg reflector (DBR). The AlAs/GaAs DBR produces >99% reflectivity over ~100 nm, centered at 1550 nm. The absorber layer consists of six InGaAs quantum wells (λ ~ 1580 nm) centered within the half-wave layer for maximum interaction with the standing wave formed by the mirror.

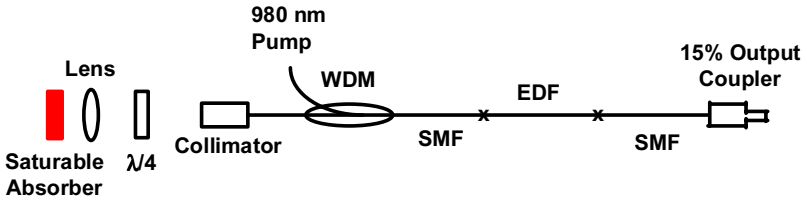

Figure 26: Diagram of fiber laser. Wavelength Division Multiplexer (WDM), Erbium Doped Fiber (EDF), Single-Mode Fiber (SMF).

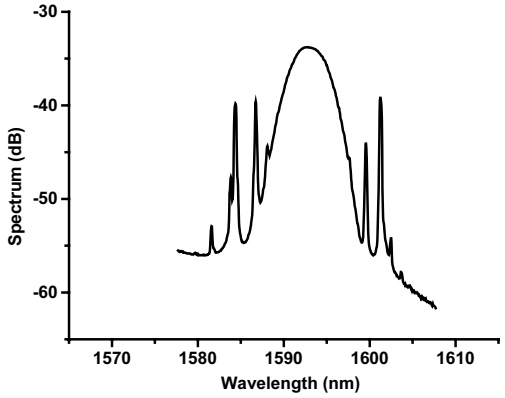

Figure 27: Optical spectrum obtained for anomalous dispersion operation.

The net dispersion of the laser cavity, shown in Figure 26, was controlled by changing the amount of anomalous dispersion fiber (SMF-28) relative to the amount of normal dispersion fiber (EDF).

The fluence incident on the absorber was varied by changing the focal length of the focusing lens as well as the intracavity power. When the cavity was adjusted for a round-trip dispersion of -0.133 ps^2, the laser would self-start to produce a single pulse with the spectrum shown in Figure 27. The full width at half maximum of the spectrum was 4.84 nm. The spectrum exhibits considerable sideband structure. Kelly sidebands are present as well as polarization sidebands, which appear to be related to the rotating polarization state at the output of the laser. As with other soliton lasers, multiple pulses were generated as the pump power was increased.

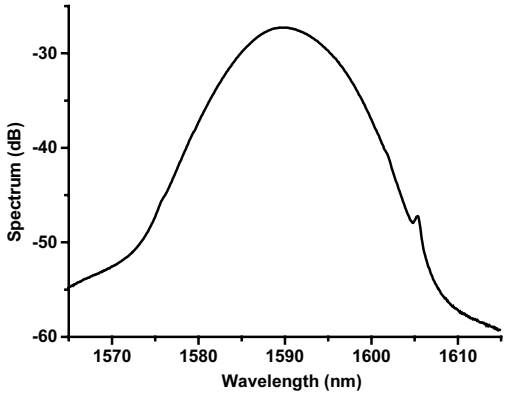

Figure 28. Optical spectrum obtained for slightly positive dispersion operation.

The round-trip dispersion of the laser was modified to +0.007 ps^2 by reducing the amount of SMF-28 in the cavity. Again modelocking was self-starting, and the spectrum of Figure 28 with a full width at half maximum of 10.95 nm was produced by single pulse per roundtrip operation. At this dispersion the sideband structure is considerably reduced and the bandwidth broadened. The dependence of the spectral width on the dispersion of the cavity and the reduction of sidebands are similar to the effects observed in stretched pulse P-APM ring lasers. Further studies of the dependence of the pulses on the saturable absorber characteristics and dispersion maps will be performed.

15 High Fluence Reflectivity Dynamics of Semiconductor Saturable Absorber Mirrors

Sponsors

US Air Force Office of Scientific Research
Grant F4920-98-1-0139
Air Force Office of Scientific Research (Defense Advanced Research Projects Agency)
Grant F49620-96-0126

Project Staff

Erik R. Thoen, Elisabeth M. Koontz, Dr. Markus Joschko, Dr. Patrick Langlois, Dr. Franz X. Kärtner, Professor Erich P. Ippen, Professor Leslie A. Kolodziejski

Starting dynamics in mode-locked lasers and Q-switched mode-locking using semiconductor saturable absorber mirrors often produce pulses with energy densities well above the saturation fluence of the absorber. Therefore it is important to characterize the absorption dynamics of such mirror structures under high fluence excitation. We have performed a detailed investigation of InGaAs/InP saturable absorber mirrors that reveals the presence of both two-photon absorption (TPA) and nonlinear free-carrier absorption (FCA), even at moderate excitation fluences. Thus, TPA and FCA may have important implications for the mode locking of lasers.

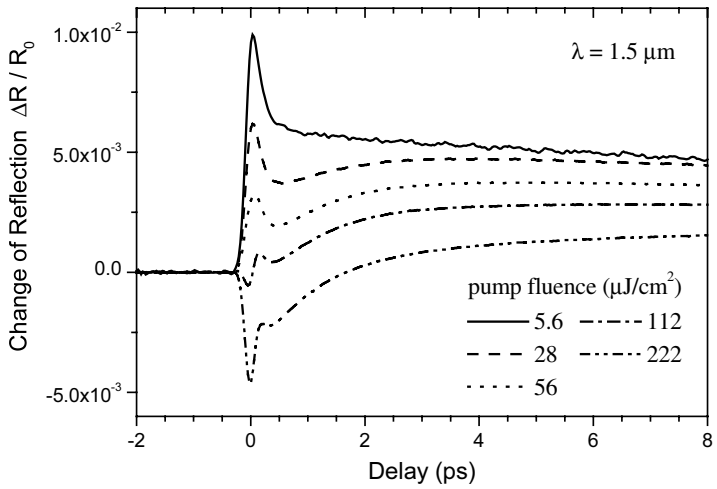

Figure 29: Differential reflectivity measurements as a function of excitation fluence at 1.50 μm. At low fluence, the bleaching dynamics of the QWs are dominant. At higher fluences, TPA and FCA develop and eventually dominate the ultrafast dynamics.

Differential reflectivity measurements at λ =1.50 μm, are presented as a function of excitation fluence, in Fig. 29, for an absorber that contains four QWs (λ ~ 1.53 μm) located at the center of the InP $\lambda / 2$ layer. Three different regimes are clearly identified in the data. First, at all pump fluences up to the 5.6 μJ/cm^2 shown, the pump-probe trace shows a fast bleaching component followed by a slow component reflecting the change in carrier density. This signature is typical for low fluence absorption dynamics of semiconductor saturable absorber structures. The fast component is attributed to spectral hole burning (SHB), with a time constant on the order of the pulse cross-correlation (~200 fs). On a longer time scale, the slow component decays with a time constant of ~50 ps, which is most likely due to carrier capture in defect states. At higher fluences (~28 μJ/cm^2), an additional component sets in that reduces the differential reflectivity, and decays with a time constant of ~1 ps, consistent with the cooling dynamics of hot carriers in the QWs. Possible mechanisms for this component are nonequilibrium free-carrier absorption (FCA) and a delayed bleaching corresponding to carrier cooling. At higher fluence levels, TPA in both the QWs and the InP layer continues to increase, and eventually, TPA and FCA dominate the ultrafast dynamics.

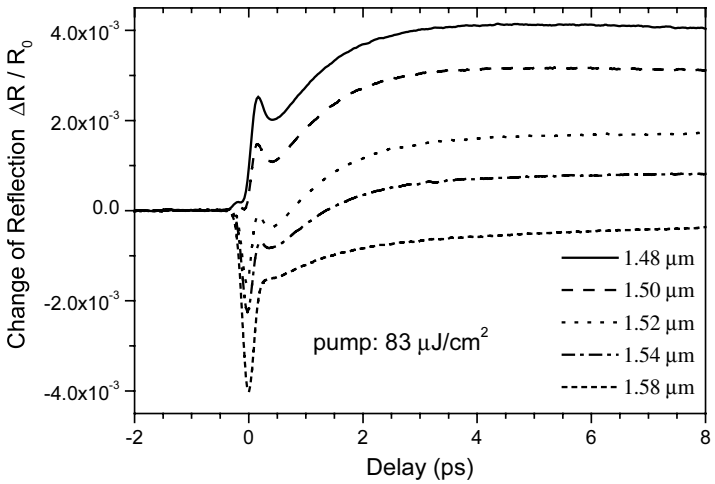

Figure 30: Differential reflectivity measurements under high fluence excitation as a function of wavelength. The wavelength is tuned from above to below the QW bandgap. Below the QW bandgap, TPA and FCA in InP are dominant.

Figure 30 depicts differential reflectivity measurements taken under moderate fluence excitation as a function of wavelength. The most significant behavior is the vanishing of the bleaching dynamics as the excitation wavelength is varied from 1.48 μm (above the QW bandgap) to 1.58 μm (below bandgap), which is consistent with a reduction of the saturable absorption at longer wavelengths. At 1.58 μm, the signal is dominated by strong TPA followed by an induced absorption component that persists for longer delays. The decay of the induced absorption is no longer described by a single ~1 ps time constant, but rather by a combination of ~1 ps and ~5 ps components, with weighting factors that favor the ~5 ps component at longer wavelengths. The ~5 ps component is attributed mainly to FCA in the InP layer, and its time constant is believed to originate from the diffusion of the TPA-induced carriers in the InP layer. As the excitation wavelength is changed from above to below the QW bandgap, the bleaching dynamic in the QWs is reduced due to a decrease in the density of absorbing states. Therefore, TPA and FCA in InP become the dominant dynamics. However, even at 1.58 μm, there are still some carriers excited in the quantum wells as evidenced by the presence of a ~1 ps component.

These results show that the nonlinear response of a semicondcutor saturable absorber mirror can be a complex function of time and pulse energy. Implications of these different aspects to modelocked laser operation and stability are being investigated.

Publications

Joschko, M., P. Langlois, E.R. Thoen, E.M. Koontz, E.P. Ippen, and L.A. Kolodziejski. "High Fluence Ultrafast Dynamics of Hot Carriers in Semiconductor Saturable Absorber Mirrors." to be presented at the Quantum Electronics and Laser Science Conference (QELS 2000), San Francisco, CA, May 2000.

Joschko, M., P. Langlois, E.R. Thoen, E.M. Koontz, E.P. Ippen, and L.A. Kolodziejski. "Ultrafast Hot-Carrier Dynamics in Semiconductor Saturable Absorber Mirrors." Appl. Phys. Lett. Forthcoming.

Langlois, P., M. Joschko, E.R. Thoen, E.M. Koontz, F.X. Kärtner, E.P. Ippen, and L.A. Kolodziejski. "High Fluence Ultrafast Dynamics of Semiconductor Saturable Absorber Mirrors." *Appl. Phys. Lett.* 75: 3841-43 (1999).

16 Enhanced Four-Wave Mixing by Proton Bombardment of Semiconductor Optical Waveguides

Sponsors

US Air Force Office of Scientific Research
Grant F4920-98-1-0139

Project Staff

Erik R. Thoen, Dr. Joseph P. Donnelly, Dr. Stephen H. Groves, Dr. Katherine L. Hall, Professor Erich P. Ippen

All-optical wavelength conversion is a highly desirable function in wavelength division multiplexed systems. Several techniques have been used for wavelength conversion at 1.55 μm including four-wave mixing (FWM) in passive InGaAsP/InP quantum-well (QW) waveguides. In these waveguides, high FWM conversion efficiencies were obtained for short-pulse low-repetition rate operation. However, at similar pump powers continuous-wave (CW) operation was ~10 dB less efficient. The difference was attributed to an additional nonlinear loss from accumulation of photogenerated free carriers during CW operation. A theory accounting for the effect of photogenerated free carriers was developed and compared to experimental results. This model predicts that by reducing the carrier lifetime ~100x, free-carrier effects are virtually eliminated.

Proton bombardment has previously been demonstrated to reduce free carrier lifetimes in InP materials. In this work we are specifically studying the enhancement of FWM performance in single- (SQW) and multiple-quantum-well (MQW) devices by such carrier lifetime reduction. A proton bombardment schedule was chosen to maximize the proton effects in the guiding layer of the fabricated waveguides. The relative CW transmission at λ = 1.548 μm and the FWM conversion efficiency for a 10 nm wavelength shift obtained on 1-cm-long SQW bombarded and unbombarded devices are shown in Figs. 31 and 32, respectively, along with calculations using the model. Both the relative transmission and efficiency improve with dose, and for $N=1x10^{12}$ cm^{-2} the efficiency improved by >3dB at 25 mW pump power. Based on the theory, the lifetime in this guide was reduced by ~10x. Larger improvements in conversion efficiency are expected at higher pump powers and optimized proton doses. Similar improvements in relative transmission and conversion efficiency were obtained with three and five QW devices.

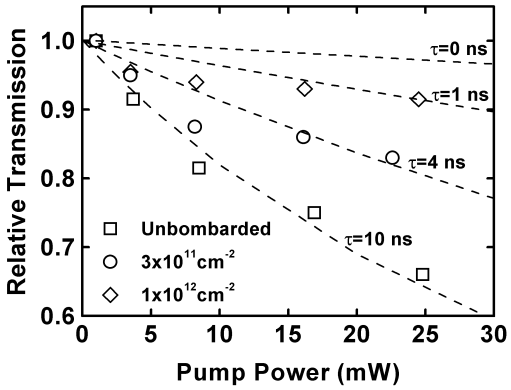

Figure 31. Relative pump transmission versus pump power measured on 1-cm-long SQW devices with proton doses as indicated. The dashed lines represent the calculated result for the indicated carrier lifetime.

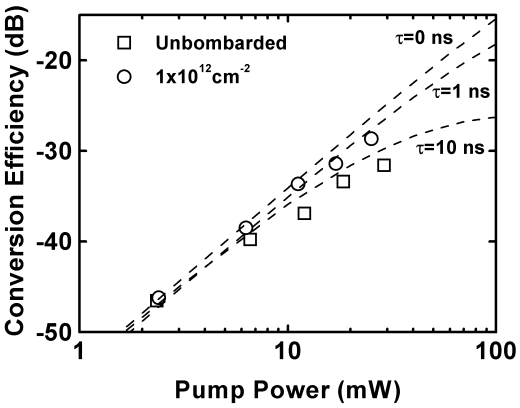

Figure 32. FWM conversion efficiency versus pump power measured on 1-cm-long SQW devices with proton doses as indicated. The dashed lines represent the calculated result for the indicated carrier lifetime.

Publications

Thoen, E.R., J.P. Donnelly, S.H. Groves, K.L. Hall, and E.P. Ippen. "Proton Bombardment for Enhanced Four-Wave Mixing in InGaAsP/InP Waveguides." *IEEE Photon. Technol. Lett*. Forthcoming.

17 Ultrafast Cr^{4+}:YAG Laser System

Sponsor

US Air Force Office of Scientific Research
Grant F4920-98-1-0139

Project Staff

Daniel Ripin, Juliet Gopinath, Serhii Zhak, Dr. Franz Kartner, Professor Erich Ippen

The Cr^{4+}:YAG laser crystal, with a broad emission bandwidth from 1.35 to 1.60 μm, is capable of generating broadly tunable light near 1.5 μm and ultrafast modelocked pulses. Such a source could be used to study modelocking dynamics, telecommunications devices, ultrafast spectroscopy, and medical imaging techniques. Room temperature operation makes Cr^{4+}:YAG an attractive alternative to cryogenically cooled color center lasers. To date, the shortest pulses produced from a Cr^{4+}:YAG laser are 43 fs[1]. In this system, the third order dispersion was not compensated; proper compensation should produce shorter pulses.

Utilizing a novel mirror design to control the third order dispersion, we are developing an ultrafast Cr^{4+}:YAG laser system. An astigmatically compensated z-fold cavity, shown in Fig. 33, produces continuous-wave (cw) lasing powers up to 0.96 W at 1450 nm, with a slope efficiency of 19.1%. The lasing wavelength is tunable from 1390 to 1490 nm. The cavity is being optimized for Kerr-lens modelocking, which will allow short pulse generation.

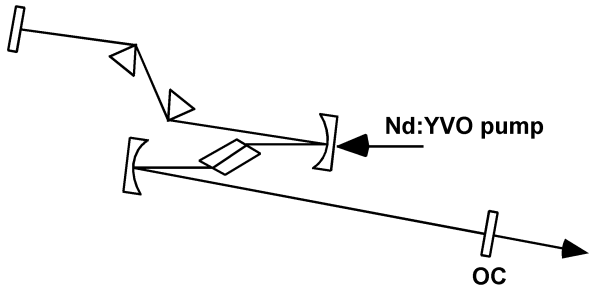

Figure 33: Cr^{4+}:YAG Laser Cavity

The system incorporates an innovative method of dispersion compensation that has not been attempted in a Cr^{4+}:YAG laser. Double-chirped dielectric mirrors[2] precisely control second and third-order intracavity dispersion, which is essential for short pulse generation. This control is achieved by chirping the thickness of both high and low index layers. Consisting of alternating SiO_2 and TiO_2 layers, these mirrors are grown with state of the art ion-beam sputtering by the group of T. Tschudi at the Institute for Applied Physics, TH Darmstadt, Germany. Intracavity calcium fluoride prisms allow fine tuning of the second and third order dispersion. Our goal of shorter pulses should be possible with this combination of novel dispersion controls incorporated into the design of the system.

References

1 Y.P. Tong, P.M.W. French, J.R. Taylor, and J.G. Fujimoto. "All-Solid-State Femtosecond Sources in the Near Infrared." *Opt. Commun.* 136: 235 (1997).

2 F.X. Kärtner, N. Matuschek, T. Schibli, U. Keller, H.A. Haus, C. Heine, R. Morf, V. Scheuer, M. Tilsch and T. Tschudi. "Design and Fabrication of Double-Chirped Mirrors." *Opt. Lett.* 22: 831 (1997).

18 Measurement of Pulse Asymmetry using Three-Photon-Absorption Autocorrelation in a GaAsP Photodiode

Sponsors

US Air Force Office of Scientific Research
Grant F4920-98-1-0139

Project Staff

Patrick Langlois, Professor Erich P. Ippen

Nonlinear optical autocorrelation is a well-established method for ultrashort pulse measurement[i]. Most recently, two-photon-absorption (2PA)-induced photoconductivity in semiconductors has become an attractive alternative to second-harmonic generation for nonlinear autocorrelation, owing to a much simpler and less expensive setup. Second-order autocorrelation methods, however, give limited information on the pulse duration and chirp. It has been shown that higher-order correlations are sensitive to pulse asymmetry. In this work we have demonstrated the use of three-photon absorption in a GaAsP photodiode for higher order nonlinear optical autocorrelation at wavelengths from 1.4 to 1.6 μm. Theoretical intensity dependence and contrast ratios are achieved and the ratio of three- to two-photon-absorption coefficient is measured. It was further demonstrated that pulse asymmetry can be measured with no direction-of-time ambiguity using unbalanced three-photon-absorption autocorrelation.

We measured pulses generated by an optical parametric oscillator with a typical duration of 150 fs and wavelength tunable from 1.4 to 1.6 μm. Two pulses with variable relative delay are focussed by an 8-mm focal-length aspheric lens to an ~8 μm spot diameter a GaAsP photodiode. The photodiode (Hamamatsu #G1115) had a bandgap around 680 nm. Hence, 3PA is expected to be the dominant nonlinear absorption mechanism at wavelengths from 1.38 to 2.07 μm. Figure 34 shows a comparison between 2PA and 3PA intensity autocorrelation measurements performed at 1.59 μm. The theoretically expected contrast ratios of 3 and 10, respectively, are obtained. The inset show the 3PA interferometric trace with its expected contrast ratio of 32.

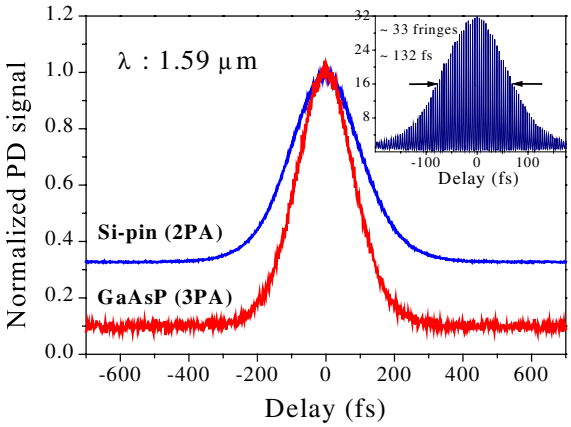

Figure 34. Measured 2PA and 3PA intensity autocorrelation traces. Inset: measured 3PA interferometric autocorrelation.

To demonstrate the capability of 3PA autocorrelation to measure asymmetric pulse shapes without direction-of-time ambiguity, we also used an unbalanced autocorrelator. Figure 35 depicts the measured 2PA and 3PA intensity autocorrelation traces of a test double-pulse measured in this manner. The delay and intensity ratio between the two ~138 fs pulses of the

test pulse are adjusted to 320 fs and 14, respectively. Their intensity ratio was 25/1. As expected, the 2PA autocorrelation trace is symmetrical and therefore cannot measure the pulse shape. However, the 3PA trace clearly reveals the double-pulse feature, and the weaker satellite pulse position relative to the main pulse is determined without ambiguity.

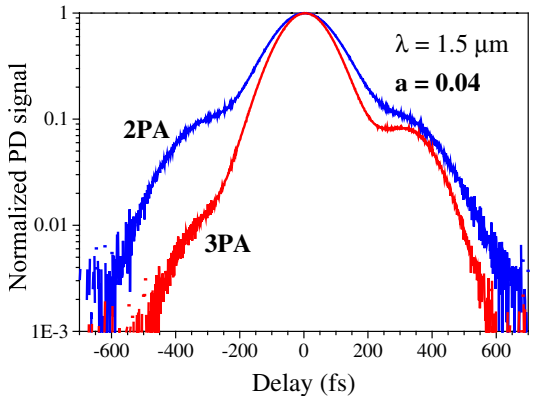

Figure 35. Measured 2PA and 3PA intensity autocorrelation traces of a test double-pulse using an unbalanced autocorrelator. The delay and intensity ratio between the two pulses of the test pulse are 320 fs and 14, respectively, for pulsewidths of ~138 fs. The intensity ratio between the two replicas at the output of the autocorrelator is *a* = 0.04.

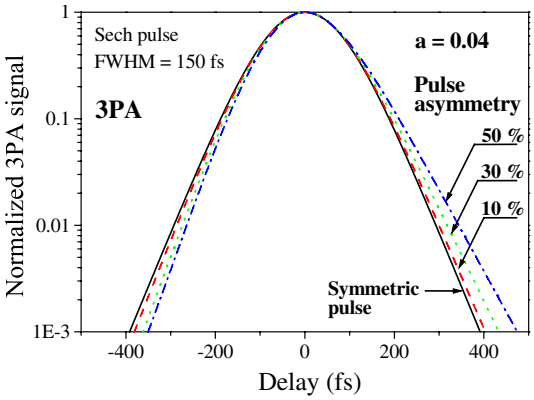

Figure 36. Calculated 3PA intensity autocorrelation traces for a $sech^2$ pulse shape using an unbalanced autocorrelator. The solid line shows the calculated trace for a symmetric pulse and the dashed, dotted and dot-dashed lines are for pulses with 10%, 30% and 50% asymmetry. The degree of asymmetry is defined in the text.

The ability for unbalanced 3PA autocorrelation to measure weaker pulse asymmetry was also investigated. Figure 36 shows calculated 3PA intensity autocorrelation traces for a sech pulse shape using an unbalanced autocorrelator with an intensity ratio of 25/1. The solid line shows the calculated trace for a symmetric pulse shape, which produces a symmetric autocorrelation trace, as expected. The dashed, dot-dashed and dotted lines are the calculated traces for a pulse asymmetry of 10%, 30% and 50%, respectively. These calculations suggest that a pulse asymmetry larger than 10% should be measurable with this method, using a high-dynamic range unbalanced 3PA intensity autocorrelation.

Publications

P. Langlois and E.P. Ippen, "Three-Photon-Absorption Autocorrelation in a GaAsP Photodiode," Conference on Lasers and Electro-Optics, 1999, Baltimore, paper CFG5.

P. Langlois and E.P. Ippen, "Measurement of Pulse Asymmetry by Three-Photon-Absorption Autocorrelation in a GaAsP Photodiode," *Opt. Lett*. 24: 1868-1870 (1999).

19 Enhanced Light Extraction from a Two-Dimensional Photonic Bandgap Light-Emitting Diode

Sponsors

US Air Force Office of Scientific Research
Grant F4920-98-1-0139
CMSE/MRSEC

Project Staff

Daniel Ripin, Alexei Erchak, Shanhui Fan, Dr. Gale Petrich, Professor Erich P. Ippen, Professor John D. Joannopoulos, Professor Leslie A. Kolodziejski

Photonic crystals, materials with a spatially periodic refractive index, have photonic density-of-states modified from free space. A frequency range over which no optical modes exist within the crystal is called a photonic bandgap (PBG). Light sources with emission frequencies inside the PBG will exhibit a suppressed spontaneous rate of decay. These two-dimensional photonic crystals with a PBG can be used to eliminate planar waveguide modes that compete with vertical emission in semiconductor LEDs. Theory predicts that elimination of these lossy planar guiding modes will be accompanied with an increase in the power of forward emission[1]. To demonstrate this effect we have fabricated a InGaP/InGaAs quantum well LED, with emission centered around 980 nm. A two-dimensional photonic crystal microstructure is then created fabricated within the LED by electron beam lithography, and is designed to inhibit waveguide modes at the emission frequency. Surface normal photoluminescence (PL) is observed to increase by as much as a factor of 10 in the photonic crystal region compared to regions on the same LED structure without photonic crystals.

The two-dimensional photonic crystal LED consists of an InGaP/InGaAs active quantum well region, a low refractive index Al_xO_y spacer layer, and an Al_xO_y/GaAs distributed bragg reflector (DBR) with a calculated stop band from 800 nm to 1400 nm. The structure is fabricated using gas source molecular beam epitaxy, direct-write electron beam lithography, reactive-ion etching, and oxidation processes.[2] The two-dimensional photonic crystal consists of a triangular lattice of holes etched within the upper InGaP cladding layer, with a nominal hole-to-hole spacing of 315 nm and a nominal hole diameter of 220 nm. The holes do not penetrate into the InGaAs quantum well layer, to avoid creating additional non-radiative surface recombination. Each two-dimensional photonic crystal LED is a 12.5 m by 12.5 μm region within a 50 μm by 50 μm LED mesa. Structure schematics and scanning electron micrographs of a structure are shown in Fig. 37.

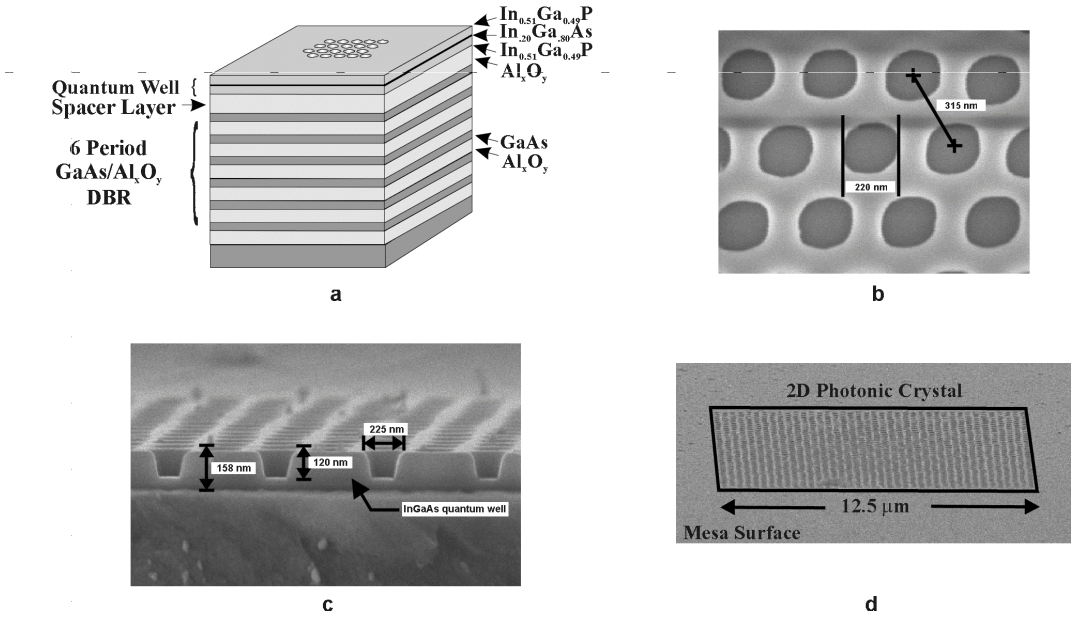

Figure 37. a) Schematic of a InGaP/InGaAs2-D PBG LED structure. b) A scanning electron micrograph (SEM) of the triangular lattice of holes forming the photonic crystal. c) Cross sectional SEM of 2-D PBG LED structure. d) SEM of the entire 2-D photonic crystal array.

Room temperature PL spectroscopy is performed with a cw 810 nm Ti:Al_2O_3 pump laser focused by a microscope objective to a 6 μm spot size on the sample. The pump is absorbed by the InGaAs quantum well layer, but prevented frm reaching the GaAs substrate by the underlying DBR. The PL is collected by the same microscope objective, and spectrally resolved by a monochromator. A sample containing a number of LED mesas is translated in 1 m step sizes with respect to the pump beam to study the PL with spatial resolution. The PL intensities are shown in Fig. 38 above a schematic of the line scan trajectory. The lowest trace shows the GaAs PL collected with the monochromator tuned to 890 nm. The GaAs PL is observed in the region between the LED mesas, and reduced in the regions with LED mesas. In the mesa region, the DBR layers reflect the pump light, preventing excitation of the GaAs substrate. The middle trace shows the same line scan, but with the spectrometer tuned to the LED emission wavelength, 980 nm. The PL signal increases in the LED regions, as expected. The top trace shows a line scan at 980 nm through mesas containing photonic crystals. The first mesa has no photonic crystal, while all subsequent mesas have a photonic crystal region embedded within the larger LED mesa. The top trace exhibits both the onset of emission over the 50 μm LED region as well as a narrower peak corresponding to the position of the photonic crystal. Enhancements of the surface normal PL intensity in the photonic crystal region compared to the background LED mesa PL as high as 10 are observed.

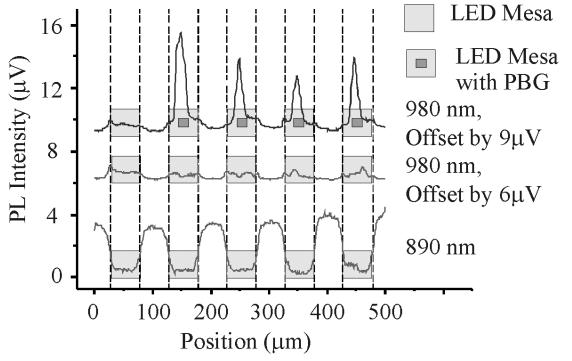

Figure 38. Spatially resolved photoluminescence (PL), taken by translating the 2-D PBG LED sample with respect to the pump beam over a line scan trajectory shown schematically below each trace. The PL in the lower, middle, and top trace are from the GaAs substrate, quantum well mesas without photonic crystals, and a line scan that passes through one mesa without a photonic crystal, and 4 mesas with a photonic crystal respectively.

Publications

A.A. Erchak, D.J. Ripin, S. Fan, G.S. Petrich, J.D. Joannopoulos, L.A. Kododziejski, and E.P. Ippen, “Increased Light Extraction from a Light-Emitting Diode using a Two Dimensional Photonic Crystal,” to be presented at the Conference on Lasers and Electro-Optics (CLEO 2000), San Fracisco, CA, May 2000.

References

1 S. Fan, P. R. Villeneuve, and J. D. Joannopoulos, "High Extraction Efficiency of Spontaneous Emission from Slabs of Photonic Crystals," *Phys. Rev. Lett.*, 78: 3294 (1997).

2 See RLE Progress Report 142, L. A. Kolodziejski.